Optics Letters

Design of nano-groove photonic crystal cavities in lithium niobate

Yihang Li,[1,2,†] Cheng Wang,[1,*,†] and Marko Loncar[1,3]

[1]*School of Engineering and Applied Sciences, Harvard University, 29 Oxford Street, Cambridge, Massachusetts 02138, USA*
[2]*Department of Electronic Engineering, Tsinghua University, Beijing 100084, China*
[3]*e-mail: loncar@seas.harvard.edu*
Corresponding author: chengwang@seas.harvard.edu

We propose a novel design of photonic-crystal nanobeam cavities in lithium niobate (LN) for both TE and TM modes, addressing problems associated with tilted sidewalls, which commonly result from dry etching. Using optimized periodical nano-groove structures, the proposed devices could achieve quality factors as high as 3.9×10^6 with a modal volume of 5.0 $(\lambda/n)^3$. We also show that such a design is promising for applications in nonlinear optics by theoretically predicting the efficiencies for electro-optic modulation and second-harmonic generation. The proposed nano-groove structures and design rules could also be applied for other material platforms that possess tilted sidewalls. © 2015 Optical Society of America

Photonic crystal (PhC) cavities have made great progress in the past decade, both theoretically and experimentally [1–5]. Thanks to their wavelength-scale modal volumes and high quality factors (Q factors), power and field could be strongly enhanced within these cavities. In particular, PhC nanobeam cavities (PCNC), in which light is confined by total internal reflection in two directions, have recently emerged as a promising platform for various applications including optomechanics [6], nonlinear optics [7,8], biosensing [9], and quantum optics [10]. Lithium niobate (LiNbO$_3$, LN) is an excellent nonlinear optical material that has been widely used for electro-optic (EO) modulation and wavelength conversion [11,12]. It is of great interest due to a high diagonal second-order susceptibility ($d_{33} = 41.7$ pm/V) [13]. In recent years, several LN nanophotonic devices based on LN thin-film technology have been reported, including whispering-gallery-mode (WGM) resonators [14–17] and photonic crystal cavities [18,19]. These results have provided fascinating opportunities to develop highly efficient nonlinear optical devices in LN using micro-cavity-enhanced

processes that have already been demonstrated in other materials [8,20]. While the Q-factors of LN WGM micro-resonators have exceeded 100,000 [15–17], the two reported 2D LN PhC cavities still suffer from low Q-factors (<500) [18,19]. The lower refractive index of LN ($\sim$2.2) [13] compared with silicon ($\sim$3.5) significantly reduces the size of the photonic bandgap, making it hard to design and fabricate robust 2D PhC cavities in LN. On the other hand, PCNCs could possibly provide much higher Q-factors since better lateral confinement of light could be achieved [21,22]. Lately, our group has developed simple and robust fabrication methods to produce various LN nanostructures with minimized surface roughness and optical scattering loss [16]. However, the post-etching nonvertical sidewalls, which are shown in Fig. 1(c), have so far prevented the implementation of conventional air-hole PCNC designs to our LN platform.

In this Letter, we propose a new scheme for LN PCNCs based on periodical nano-grooves. Our nanobeam cavitiy design offers Q-factors over 10^6 for both TE and TM modes while maintaining modal volumes $\sim$5 and 10 $(\lambda/n)^3$, respectively. The nano-groove structures are constructed such that all sidewalls make an angle $\theta = 35°$ with respect to the vertical direction, which is determined from our fabrication results. We also demonstrate that our LN PCNCs could potentially achieve EO modulation with a switching voltage $\sim$1.4 V and a SHG efficiency around 1800%/W.

The principle of designing an ultrahigh-Q PCNC is to linearly increase the mirror strength on both sides of the cavity,
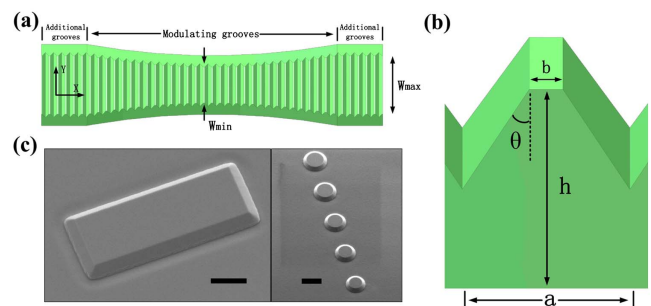

Fig. 1. Schematics of photonic crystal nano-groove cavities. (a) Top view. (b) Cross-sectional view on x–z plane. (c) SEM images of typical fabricated LN nanostructures with tilted sidewalls. Scale bar: 1 μm.

by carefully engineering system parameters, so as to achieve a Gaussian-like field profile [4]. However, as is mentioned before and shown in Fig. 1(c), the tilted sidewalls caused by dry etching will turn the conventional cylindrical or square air-holes into conical holes, severely reducing the size of the bandgap. To maintain sufficient mirror strength, we use nano-groove structures to replace air-holes, shown schematically in Fig. 1. The groove width, depth, and period are kept constant over the entire structure, while beam width is quadratically increased. Additional grooves with fixed beam width at both ends of the cavity are used in the TM case.

All simulations in this Letter were performed using a 3D finite-difference time-domain (FDTD, Lumerical) method. The LN crystal orientation is chosen to be z-cut, such that $n_z = n_e = 2.13$ and $n_x = n_y = n_o = 2.21$ [13]. The corresponding nonlinear coefficients used in the following simulations are $r_{33} = 30.9$ pm/V (EO modulation) and $d_{33} = 41.7$ pm/V (SHG) [13]. Since the thickness of the thin LN film we use (400 nm) is smaller than wavelength, we start with TE modes that possess higher effective indices than TM modes. A typical TE band diagram of a nano-groove photonic crystal is shown in Fig. 2(a) (red line), with period $a = 450$ nm, $b = 50$ nm for a groove width of 400 nm, and beam width $W_{min} = 550$ nm. At the edge of the first Brillouin zone, the corresponding frequency is 195 THz (1538 nm), and we take this set of parameters for the cavity mode. As the device extends into the mirror region, the beam width is quadratically increased to $W_{max} = 900$ nm. In this case, no additional grooves are used. The TE band diagram at the end of the mirror region is shown as the black line as Fig. 2(a), such that our operating frequency is right in the center of the bandgap.

Figure 2(b) demonstrates the Q-factors and modal volumes of such cavities with different numbers of mirror groove pairs. As the groove number increases, Q-factors grow exponentially, and modal volumes grow linearly. With 80 mirror groove pairs, an ultrahigh-Q-factor of 3.9×10^6 is achieved. The corresponding modal volume is 5.0 $(\lambda/n)^3$. Figure 2(c) shows the corresponding Gaussian-like field distribution of our LN nanobeam cavities. We have also simulated the case where the actual sidewall angle differs from the nominal value. Results show that, within $\pm 5°$ angle variations, the aforementioned Q-factor could maintain above 3.1×10^5, and the operating wavelength fluctuation is within ± 25 nm.

For nonlinear optical applications using z-cut LN on insulator substrates, it is appealing to use TM modes, so as to take advantage of the largest nonlinear coefficient component $\chi^{(2)}_{zzz}$. While TM modes are favored in high-aspect-ratio beams [23], their designs are challenging in a 400-nm-thin film since the lowered effective index leads to a smaller bandgap. To compensate for the weakened bandgap effect and increase the effective index, the period and the groove width are increased. The final parameters are chosen as: $a = 485$ nm, $b = 50$ nm, $W_{min} = 470$ nm, $W_{max} = 900$ nm. The corresponding band diagrams are shown in Fig. 3(a), indicating an operating frequency of 199 THz (1508 nm).

It should be noted that the 2nd-order TE dielectric band [green line in Fig. 3(a)] is close to the operating frequency, and it could cause detrimental loss channels. It shares the same symmetry and has finite field overlap with the 1st-order TM mode. We have carefully avoided the case where the 2nd-order TE dielectric band edge intersects with the operating frequency in the mirror region by engineering system parameters. In this case, we achieved a Q-factor of 1.8×10^6 with 100 pairs of modulating grooves. Modal volumes of TM-mode cavities are larger than those in TE cases, varying from 9 to 15 cubic wavelengths, due to weaker Bragg confinement in x direction and more field leakage in z direction caused by lower effective indices. Figure 3(d) shows the field distribution in x–z plane. The electric field jumps up as it passes through the top and bottom edges of the beam, following the required boundary conditions. However, most of the energy (>70%) is still confined in the beam as expected.

Additional grooves with fixed beam width at each end of the modulating parts could be used to further strengthen the light confinement in x direction and increase the Q-factors while maintaining similar levels of modal volumes, shown in Fig. 3(b). With 70 modulating grooves and 20 additional grooves on each side, the Q-factor (1.5×10^6) is comparable

Fig. 3. (a) TM band diagrams in the cavity and mirror regions, as well as the 2nd-order TE band in the mirror region. (b) Theoretical Q factors, modal volumes, and transmissions (T) with different numbers of modulating groove pairs and additional groove pairs. (c) E_z distribution in x–y plane at the top of the beam. (d) E_z distribution in x–z plane at the center of the beam. Black lines show the outline of the device.
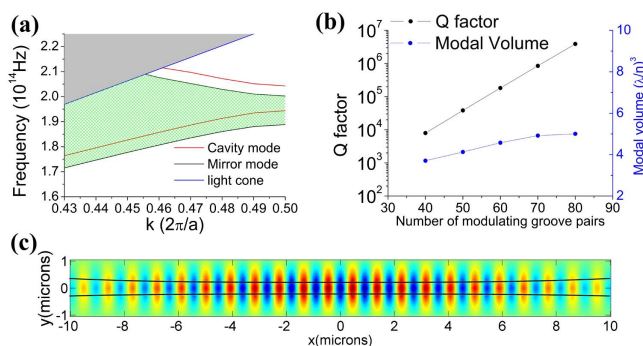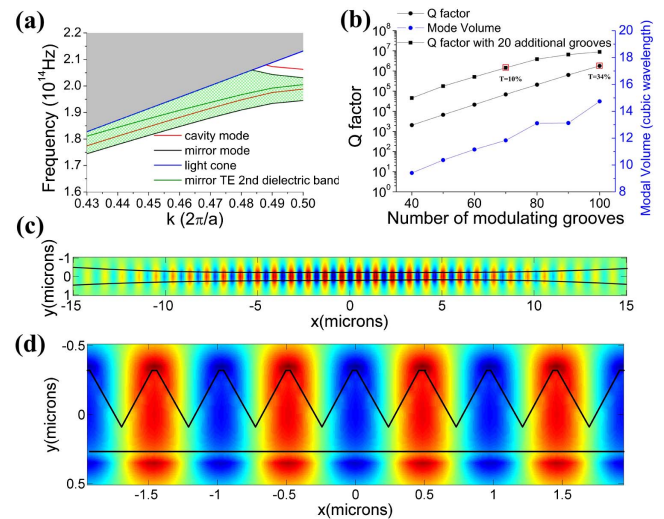
Fig. 2. (a) TE band diagrams for cavity and mirror modes. (b) Theoretical Q-factors and modal volumes with different numbers of modulating groove pairs. (c) E_y distribution in x–y plane at the top of the beam. Black lines show the outline of the device.

with the case of 100 modulating grooves, while its modal volume (11.8 $(\lambda/n)^3$) is 20% smaller. In this case, however, radiation loss starts to dominate over waveguide coupling loss, which lowers the cavity transmission ($T = 10\%$, as compared with 34% in the 100 modulating pairs case).

With small footprints and high-Q-factors, our LN PCNCs could be used to realize compact on-chip EO modulators with low switching voltages. From FDTD simulations, the refractive index sensitivity of our device was calculated to be $\Delta f/\Delta n = 28.5$ THz/RIU (refractive index unit) or $\Delta\lambda/\Delta n = 218$ nm/RIU. Here we assume the same scheme and structural parameters used in [14], where the LN device layer is sandwiched between 0.85-µm top oxide and 2.5-µm bottom BCB. The relation between applied voltage and resulting electric field within the LN beam could be estimated using a parallel capacitor model ($\varepsilon_{LN} = 28$, $\varepsilon_{SiO2} = 3.8$, $\varepsilon_{BCB} = 2.6$) [14]. A frequency tunability of 0.13 GHz/V could be achieved, which is comparable with the theoretical value in [14], but realized within a much smaller footprint. Moreover, the high Q-factors significantly reduce the required voltage to switch the cavity between on and off states. In the case of 100 groove pairs, a Q-factor as high as 1.4×10^6 could be maintained with the existence of metal electrodes. Here the electrodes are pushed further away (3-µm silicon dioxide layers on both sides of the device), and a switching voltage as low as ~1.4 V is expected to be achieved.

The field enhancement in our ultrahigh-Q nanobeam cavities also leads to a dramatic enhancement in nonlinear optical responses. Here we take SHG as an example and simulate the SHG response using nonlinear FDTD simulations. A continuous-wave mode source (oscillating at the cavity resonance frequency) was used to pump the system from one waveguide port. Simulation time was set to be sufficiently long so that a steady state was reached with constant output SHG power. The output power was monitored in all directions so as to capture the total internally generated SHG power. Using this method, the conversion efficiencies for 40, 45, and 50 mirror groove pairs were calculated and shown as the red stars in Fig. 4(a).

These results are valid in the limit of low conversion where spontaneous down conversion and pump depletion are negligible. Since the device is singly resonant (SHG wavelength is off resonance), the conversion efficiency (normalized by input power) is quadratically dependent on the intra-cavity power, or $\sim(QT^{0.5}/V)^2$, where T is the cavity transmission, and V is the modal volume, which could be derived from the temporal coupled-mode theory [24]. Using this relation, we numerically predicted the SHG efficiencies for the cases of 45 and 50 mirror pairs [blue spots in Fig. 4(a)] based on the efficiency of 40 groove pairs, which match well with 3D nonlinear FDTD sim-

ulation results. For groove pair numbers larger than 50, corresponding conversion efficiencies were also predicted and shown in Fig. 4(a). With a Q-factor ~10^6 (100 groove pairs), the total second-harmonic power radiated in all directions yields a SHG efficiency of 1800%/W theoretically. Since the coupling of SHG light into the waveguide ports is not optimized, most SHG light is free-space radiated. Figure 4(b) shows the far-field analysis of second-harmonic radiation from the top of the device. An objective lens with NA = 0.65 would be able to collect 31% of the internally generated SHG power, which corresponds to an efficiency of 560%/W.

In conclusion, we have demonstrated the design of ultrahigh-Q photonic crystal cavities in LN for both TE and TM modes. Novel nano-groove structures were optimized for tilted sidewalls commonly resulting from the dry etching of LN. Q-factors as high as 3.9×10^6 with a modal volume of 5.0 cubic wavelengths could be achieved, representing more than 3 orders of magnitude improvement over previous reports on similar platforms [18,19]. We have also numerically calculated our cavities' performance for on-chip EO modulation and wavelength conversion applications. We show that our devices could theoretically achieve an EO modulation voltage as low as 1.4 V and an internal SHG efficiency of 1800%/W. Moreover, our nano-groove design could also be applied in other material systems and fabrication platforms with nonvertically etched sidewalls, e.g., TiO$_2$ [25], SiO$_2$ wet etching.

Fig. 4. (a) SHG efficiencies for different groove pair numbers using nonlinear FDTD (red stars) and numerical prediction (blue spots). (b) Farfield analysis of scattered SHG light.

REFERENCES

1. S. Y. Lin, J. Fleming, D. Hetherington, B. Smith, R. Biswas, K. Ho, M. Sigalas, W. Zubrzycki, S. Kurtz, and J. Bur, Nature **394**, 251 (1998).
2. Y. Akahane, T. Asano, B. S. Song, and S. Noda, Nature **425**, 944 (2003).
3. J. Vuckovic, M. Loncar, H. Mabuchi, and A. Scherer, IEEE J. Quantum Electron. **38**, 850 (2002).
4. Q. Quan and M. Lončar, Opt. Express **19**, 18529 (2011).
5. P. B. Deotare, M. W. McCutcheon, I. W. Frank, M. Khan, and M. Lončar, Appl. Phys. Lett. **94**, 121106 (2009).
6. P. B. Deotare, I. Bulu, I. W. Frank, Q. Quan, Y. Zhang, R. Ilic, and M. Lončar, Nat. Commun. **3**, 846 (2012).
7. I. B. Burgess, Y. Zhang, M. W. McCutcheon, A. W. Rodriguez, J. Bravo-Abad, S. G. Johnson, and M. Loncar, Opt. Express **17**, 20099 (2009).
8. S. Buckley, M. Radulaski, J. Petykiewicz, K. G. Lagoudakis, J.-H. Kang, M. Brongersma, K. Biermann, and J. Vučković, ACS Photonics **1**, 516 (2014).
9. Q. Quan, D. L. Floyd, I. B. Burgess, P. B. Deotare, I. W. Frank, S. K. Tang, R. Ilic, and M. Loncar, Opt. Express **21**, 32225 (2013).
10. J. Thompson, T. Tiecke, N. de Leon, J. Feist, A. Akimov, M. Gullans, A. Zibrov, V. Vuletić, and M. Lukin, Science **340**, 1202 (2013).
11. E. L. Wooten, K. M. Kissa, A. Yi-Yan, E. J. Murphy, D. A. Lafaw, P. F. Hallemeier, D. Maack, D. V. Attanasio, D. J. Fritz, and G. J. McBrien, IEEE J. Sel. Top. Quantum Electron. **6**, 69 (2000).
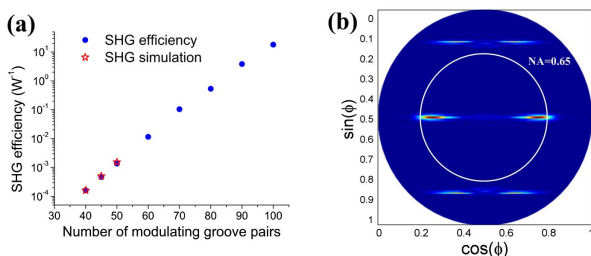
12. G. Miller, R. Batchko, W. Tulloch, D. Weise, M. Fejer, and R. Byer, Opt. Lett. **22**, 1834 (1997).
13. D. N. Nikogosyan, *Nonlinear Optical Crystals: A Complete Survey* (Springer, 2006).
14. A. Guarino, G. Poberaj, D. Rezzonico, R. Degl'Innocenti, and P. Günter, Nat. Photonics **1**, 407 (2007).
15. R. Wang and S. A. Bhave, arXiv preprint arXiv:1409.6351 (2014).
16. C. Wang, M. J. Burek, Z. Lin, H. A. Atikian, V. Venkataraman, I. C. Huang, P. Stark, and M. Lončar, Opt. Express **22**, 30924 (2014).
17. J. Lin, Y. Xu, Z. Fang, M. Wang, J. Song, N. Wang, L. Qiao, W. Fang, and Y. Cheng, Sci. Rep. **5**, 8072 (2015).
18. J. Dahdah, M. Pilar-Bernal, N. Courjal, G. Ulliac, and F. Baida, J. Appl. Phys. **110**, 074318 (2011).
19. S. Diziain, R. Geiss, M. Zilk, F. Schrempel, E. B. Kley, A. Tünnermann, and T. Pertsch, Appl. Phys. Lett. **103**, 051117 (2013).
20. C. Xiong, W. Pernice, K. K. Ryu, C. Schuck, K. Y. Fong, T. Palacios, and H. X. Tang, Opt. Express **19**, 10462 (2011).
21. M. Khan, T. Babinec, M. W. McCutcheon, P. Deotare, and M. Lončar, Opt. Lett. **36**, 421 (2011).
22. Q. Quan, I. B. Burgess, S. K. Tang, D. L. Floyd, and M. Lončar, Opt. Express **19**, 22191 (2011).
23. Y. Zhang, M. W. McCutcheon, I. B. Burgess, and M. Lončar, Opt. Lett. **34**, 2694 (2009).
24. J. D. Joannopoulos, S. G. Johnson, J. N. Winn, and R. D. Meade, *Photonic crystals: molding the flow of light* (Princeton University, 2011).
25. J. D. Bradley, C. C. Evans, J. T. Choy, O. Reshef, P. B. Deotare, F. Parsy, K. C. Phillips, M. Lončar, and E. Mazur, Opt. Express **20**, 23821 (2012).